Continuum Variability of Active Galactic Nuclei in the Optical-UV Range

Dario Trèvese[1]

Dipartimento di Fisica, Università di Roma “La Sapienza”,

Piazzale A. Moro 2, I-00185 Roma (Italy), trevese@uniroma1.it

Richard G. Kron[1]

Fermi National Laboratory, MS 127, Box 500,

Batavia, IL 60510, rich@oddjob.uchicago.edu

and

Alessandro Bunone

Dipartimento di Fisica, Università di Roma “La Sapienza”,

Piazzale A. Moro 2, I-00185 Roma (Italy)

Received ______________________; accepted ______________________

[1]Visiting Astronomer, Kitt Peak National Observatory, National Optical Astronomy Observatories, which is operated by the Association of Universities for Research in Astronomy, Incorporated, under cooperative agreement with the National Science Foundation

ABSTRACT

The variability of the continuum spectral energy distribution has been analyzed for a complete magnitude-limited sample of quasars in Selected Area 57, observed at two epochs in the photographic U, B_J, F and N bands with the Mayall 4m telescope at Kitt Peak. Changes $\delta\alpha$ of the spectral slope α appear correlated with brightness variations $\delta log f_\nu$ indicating an average hardening of the spectrum in the bright phases. This confirms that the correlation of variability with redshift, found in a single observing band, is due to intrinsic spectral changes. The average observed $\delta\alpha - \delta log f_\nu$ relation is consistent with the spectral change due to temperature variation of a black body of about $2.5 \cdot 10^4 K$.

Subject headings: galaxies: active - galaxies: multicolor photometry - galaxies: Seyfert - photometry : variability - quasars: general

1. Introduction

Variability provides a powerful tool for constraining the physics of Active Galactic Nuclei. The original models based on a central black hole surrounded by an accretion disk (Rees 1984) were based on the constraints on the source size and energy density provided by the early single-band variability studies. Single-epoch multi-wavelength observations, covering simultaneously the range from radio to gamma-ray frequencies, are of crucial importance in suggesting the physical mechanisms responsible for the emission. However, in general they cannot sufficiently constrain the large number of parameters involved in models. So far multi-wavelength monitoring, with adequate time sampling and duration, has been possible for a small number of low-redshift objects, thanks to large international collaborations (see the review of Ulrich, Maraschi, and Urry 1997 and refs. therein). These observations provided further clues to and constraints on the radiation processes and reprocessing mechanisms, since changes of the spectral energy distribution (SED) associated with flux variations can be interpreted in terms of an interplay of emission components of different spectral shape and variability properties. Various classes of active galactic nuclei (AGN) show different variability properties. Blazars show strong ($> 1\ mag$) variations of the observed fluxes on time scales from days to months from radio to gamma frequencies, while in the optical-UV Seyfert 1 and normal quasars (QSOs) show smaller ($< 0.5\ mag$) variability on time scales greater than a few months, although $> 1\ mag$ variations on time scales of days have been detected in X-rays in some Seyfert galaxies (Mushotzki et al. 1993 and refs. therein) (in the following we ignore the traditional distinction at M_B=-23 between Seyfert 1 galaxies and QSOs). The result of multi-frequency monitoring indicates that the optical-UV continuum of AGNs hardens during the bright phases (Cutri et al. 1985, Edelson et al. 1990, Kinney et al. 1991, Paltani and Courvoisier 1994) in the near infrared-optical-UV range, while little or no correlation is thought to be present in BL Lac objects(Edelson 1992, see however Massaro et al. 1996).

Optical observations at faint magnitudes ($B \approx 20 - 23\ mag$) enable magnitude-limited statistical samples to be constructed (mostly of radio-quiet objects) in a single field of a large telescope, and repeated broad-band imaging provides light curves for each AGN in the sample (Hawkins 1983, Koo & Kron 1988, Trèvese et al. 1989(T89), Trèvese et al. 1994(T94), Cristiani, Vio, & Andreani 1990, Hawkins & Véron 1993, Hawkins & Véron 1996, Bershady, Trèvese & Kron 1998(BTK98)) allowing the ensemble variability properties of the sample to be assessed.

Studies of this kind are complicated by the fact that in all magnitude-limited samples the luminosity is strongly correlated with redshift (L-z correlation), since the majority of objects lie close to the limiting flux. This makes it difficult to isolate the intrinsic variability-luminosity (v-L) and variability-redshift (v-z) correlations.

Since early studies, the relation between absolute optical luminosity and optical variability has been addressed by several authors (Angione & Smith 1972, Uomoto et al. 1976, Pica & Smith 1983), with the aim of discovering whether QSOs are made up of multiple sources or single coherent sources. In the former case, a decrease of variability amplitude with luminosity is expected. In recent years, consensus has progressively grown that brighter QSOs are less variable on average (Trèvese et al. 1994(T94),Hook et al. 1994, Cristiani et al. 1996) (see Giveon et al. 1999 for a recent summary). This would seem to support a model where the active nucleus is powered by a series of supernova explosions Aretxaga & Terlavich, Aretxaga, Cid Fernandes & Terlavich, though this model can fail to reproduce the variability amplitude in the case of most luminous QSOs, according to Hawkins 2000. A similar negative correlation of X-ray variability with the 1-10 keV luminosity was found in Seyfert galaxies and QSOs and interpreted in terms of large number of incoherent flaring subunits by Green et al. 1993. On the contrary, a positive v-L correlation was found by Edelson 1992 for the Blazar population.

Concerning the L-z correlation, the situation is further complicated by the fact that the different variability indicators, used by different authors, are affected in different ways by the v-L and L-z correlation and by spurious redshift dependence due to the combination of time dilation, intrinsic variability time-scales, and total duration of the observational campaign. This led Giallongo, Trèvese & Vagnetti (1991) (GTV) to introduce a variability indicator based on the rest-frame structure function. Adopting this indicator, they found a positive correlation of variability with redshift, taking properly into account the effect of v-L and L-z correlations. This result has been subsequently confirmed by the analysis of the QSO structure function in bins of luminosity and redshift, performed by Cristiani et al. 1996 using all the statistical samples available at that time.

GTV suggested that the v-z correlation can by explained by a hardening of the spectrum in the bright phases (and vice versa), coupled with the increase of the rest-frame frequency with redshift, for a fixed observing band.

Di Clemente et al. 1996, on the basis of the analysis of various QSO samples, have shown that indeed, on average, variability increases with the rest-frame frequency. This provides an indirect statistical argument for a slope change of the quasar SED associated with luminosity variability. Moreover the increase of variability with rest-frame frequency is quantitatively consistent with the v-z correlation.

However, a direct statistical quantification of the change of spectral slope associated with luminosity variation is still missing. Moreover, even though variability has historically played a key role in constraining models of the QSO central engine, the physics of variability is still largely unknown. In fact, quite diverse variability mechanisms have been proposed, including supernovae explosions (Aretxaga & Terlavich), instabilities in the accretion disk (Kawaguchi et al. 1998), and gravitational lensing due to intervening matter (Hawkins & Véron 1993, Hawkins 2000). Discriminating between these different models on the sole basis of single band correlation functions and v-L and v-z correlations is a very difficult task.

In the present paper we analyze UB_JFN photometry of the faint QSO sample of SA57 to look for direct evidence of an average spectral hardening for increasing flux. A statistical quantification of the spectral slope changes as a function of luminosity variations provides a new constraint for models of the variability mechanism. We also discuss the consistency of the SED variations with the v-z correlation and with temperature changes of an emitting black body.

This paper is organized as follows: data and reduction procedures are described in section 2; the statistical analysis of SED changes and their relation with flux variations are described in section 3; a concluding discussion is presented in section 4.

2. The AGN Sample and the Spectral Energy Distributions

Statistical studies of variability require a QSO sample based on clearly known selection criteria, whose effects are clearly understood and quantifiable. Among the existing QSO samples, the magnitude-limited sample of faint QSOs of Selected Area 57 (Kron & Chiu 1981, Koo, Kron & Cudworth 1986(KKC)) is probably the most studied. This field has been repeatedly observed since 1974 with the Mayall 4 m telescope at Kitt Peak in the photographic U, B_J, F, N bands. Different techniques, such as colors, lack of proper motion, and variability, have been applied to search for AGNs down to $B_J = 23$ and to estimate the completeness of the sample. Spectroscopic confirmation of almost all of the QSO candidates has been obtained (Kron & Chiu 1981, Koo, Kron & Cudworth 1986(KKC),Koo & Kron 1988,T89,Majewski et al. 1991,T94), with the exception of the faint part of the sample of extended sources of BTK98. This allows for the first time to perform a statistical analysis of the variability of the spectral energy distribution of QSOs. Single-band variability studies (T89, T94, BTK98) of the AGN sample where based on the entire collection of J (or B_J) plates. However, as discussed in the next section, the most reliable analysis of SED variability is obtained considering only “simultaneous” U, B_J, F, N observations. For this reason we selected the two sets of plates taken in April 1984 and in April 1985. The list of the plates is given in Table 1, which contains plate identification, the date, and the photometric band. The effective bandwidths of the U, B_J, F, N bands are 570, 1250, 1150, 1720 Å respectively and the effective wavelengths are 3540, 4460, 5980, 7830 Årespectively.

EDITOR: PLACE TABLE 1 HERE.

Photometric methods and signal-to-noise ratio optimization are described in T89, T94 and BTK98. The AGN sample consists of 40 spectroscopically confirmed objects. Table 2 gives the photometry on each of the 9 plates considered in the present analysis.

EDITOR: PLACE TABLE **??** HERE.

Of these 40 objects, 35 are the QSOs discussed in T94, while another 5 objects are the spectroscopically confirmed AGNs selected by BTK as variable objects with extended images. The limiting magnitude of the sample is $m_2 < 23.5\ mag$, where m_2 is the B_J magnitude evaluated in a fixed aperture of radius $0''.5$ (but see BTK98 for faint extended objects). The cumulative redshift distribution has 25%, 50%, and 75% of the objects below z=(0.75, 1.16, 1.80) respectively.

EDITOR: PLACE FIGURE 1 HERE.

Figure 1 shows the Hubble diagram of the sample. Figure 2 shows a comparison of the U, B_J, F fluxes at one epoch (April 1984), normalized at $\lambda = 2000$ Å, as a function of the rest-frame frequency.

EDITOR: PLACE FIGURE 2 HERE.

Most objects have similar spectral slopes, with five main exceptions, which are objects with a much steeper spectrum. Two of them are low redshift and two are the highest redshift objects. The former two, N_{ser} 110195 with z=0.243 and N_{ser} 114264 with z=0.287, belong to the sample of BTK98 and are relatively faint AGNs, with $M_{B_J} = -19.6$ and $M_{B_J} = -20.7$ respectively. Their r.m.s. variability is among the lowest in the sample of BTK. Since we know that, in general, fainter AGNs show a stronger variability, we may argue that in this case the light from the nucleus is diluted by the stellar light of the host galaxy. This could also explain the steep spectrum. If so, the spectral changes would also be affected by the presence of a constant stellar component. Two other steep-spectrum objects are the most distant in the sample, N_{ser} 111610 with z=3.02 and N_{ser} 101392 with z=3.08, and $M_{B_J} = -20.7$ and $M_{B_J} = -24.9$ respectively (bottom right in Figure 2). Their spectral slopes are strongly affected by intergalactic Ly-α absorption. In particular the B_J band falls in the (rest-frame) region between the emission Ly-α and the Lyman-limit, and the U band falls beyond the Lyman-limit. The relevant fractional attenuation of the continuum can be evaluated as $\gtrsim$ 0.2 and and $\gtrsim$ 0.5 respectively, e.g. from Steidel & Sargent (1987). Notice that, in Figure 2, the downwards shift of the F-band flux is due to the normalization at 2000 Å computed from the extrapolation of the steep uncorrected spectrum, and is dramatically reduced if the extrapolation to 2000 Å is done after the correction for the Ly-α absorption. Once corrected for the absorption the two spectra become consistent with the average slope $\langle\alpha\rangle \approx -0.5$ of the sample (see Gaillongo, Gratton & Trèvese 1990). We stress that the changes of the spectral index due to variability are independent of the intergalactic absorption, even though the apparent SED is affected. Figure 3 shows, with arbitrary scale, the data reported in Table 2.

EDITOR: PLACE FIGURE 3 HERE.

In the majority of the cases the deviations of the SED from a linear $log f_\nu - log\nu$ relation are small, but some objects have a local maximum of emission in the observed frequency range. Of course, such a humped SED can be relevant for physical models of the emission mechanism. Correlations of colors with other properties, e.g. the X-optical slope (Miyaji et al. 1997), can be affected by artificial curvature due to non-simultaneous measures of different bands.

3. Variability of the continuum spectral energy distribution

Our aim is to correlate the SED changes with the brightness variations. We do this by correlating the variations $\delta\alpha$ of the spectral slope α, defined by $log f_\nu \propto \nu^\alpha$, with the variation of $\delta log f_\nu$, where ν is the rest-frame frequency of one of the observing bands. In order to minimize the effect of noise, we are subject to several restrictions. On average the best signal-to-noise ratio is obtained on J plates; thus we use pairs of J plates to compute $\delta log f_{\nu_J}$. The noise in α is lower for larger leverage on the $log\nu$ axis and the larger the number of bands used. The data used for computing $\delta log f_{\nu_J}$ must not be used in the calculation of α, otherwise a spurious correlation is found, namely $\delta\alpha$ and $\delta log f_{\nu_J}$ appear correlated even in the absence of variability, due to the presence of correlated noise in both $\delta\alpha$ and $\delta log f_{\nu_J}$. This statistical bias may even lead to strong and highly significant correlation (Massaro & Trèvese 1996). It must be considered also that the SED cannot be represented exactly by a power law in the wavelength range studied. This is not a problem as long as α at different epochs is computed in a similar way. In fact α is a linear combination of the values of $log f_{\nu_J}$ measured in different bands, thus any deviation of the SED from a power law, while affecting α, does not affect $\delta\alpha$, which is a linear combination of $\delta log f_{\nu_J}$ values. This is true even when the deviation from the power law is produced by a (non-variable) absorption in some of the bands. However, computing α in a very different way at two epochs, e.g. using U and N or J and F bands, can generate $\delta\alpha$ values not due to variability. This 'spurious' $\delta\alpha$ can even be different for two identical QSOs, if they have different redshifts. The above considerations led us to select the two-epoch set of plates described in Table 1, to minimize spurious effects and to increase the reliability and robustness of the results. We determined α from a linear fit in the $log f_\nu - log\nu$ plane from U, B_J, F, N data at the first epoch and from U, F, N data at the second epoch (the N magnitude of N_{ser} 104855 is missing at the first epoch). In this way two more J plates (MPF3919 and MPF3977), one at the first and one at the second epoch, are available to compute an independent δf_{ν_J}. Emission lines, which are known to vary on the same time scale of the continuum emission, may also affect the spectral slope variations. Whether they cause a positive or negative contribution to the slope depends on the particular band and redshift. Of course, if line variation were perfectly synchronous and proportional to continuum variation they would not cause any additional slope variability. A recent paper of Kaspi et al. 2000, provides light curves of $H_\alpha, H_\beta, H_\gamma$ lines and continuum of 28 PG QSOs with a sampling interval of 1-4 months for a total observing period of 7.5 years. From the line-continuum cross-correlation function the authors derive time delays of the order of 100 days for 17 of the 28 QSOs. H_α flux fluctuations are smaller than 20% of the continuum fluctuations. Continuum and line variation are, in general, strongly correlated and the time width of the cross correlation function, which depends on the power spectrum of variability, is larger than the delay. As a result, in most cases the cross-correlation at zero time-lag is large ($\gtrsim 0.5$) so that line variations synchronous and proportional to the continuum variation can be considered a good approximation for the purpose of the present analysis.

Although we cannot correlate the slope changes with flux variations for each individual object, we can study the "ensemble average" of spectral variations of the 40 objects of our sample between two epochs. In Figure 4, $\delta\alpha$ versus $\delta log f_{\nu_J}$ is reported for the entire sample, with the two linear regression lines, showing an average increase of the spectral slope α for increasing f_J, i.e. a hardening of the spectrum in the brighter phases. The distribution of $\delta\alpha$'s is symmetric about zero, indicating the absence of any strong systematic effect on the spectral slopes.

EDITOR: PLACE FIGURE 4 HERE.

The correlation coefficient between $\delta\alpha$ and $\delta log f_{\nu_J}$ is $\rho = 0.39$ and the probability of the null hypothesis is $P(>\rho) = 1.28 \cdot 10^{-2}$. We take the above result as statistical evidence for a relation of the type $\delta\alpha = a + b\ \delta log f_{\nu_J}$ between α and luminosity variations. To check the dependence of the result on the two most deviant points (N_{ser}=118122 $\Delta log f_J$=-0.276, and N_{ser}=104885 $\Delta log f_J$=0.292) we evaluated the correlation excluding in turn: i) both the points, ii) the first point and iii) the second point. We obtained respectively: i) $\rho = 0.288$ $P(>\rho) = 7.98 \cdot 10^{-2}$, ii) $\rho = 0.290$ $P(>\rho) = 7.33 \cdot 10^{-2}$ and iii) $\rho = 0.395$ $P(>\rho) = 1.29 \cdot 10^{-2}$. To determine the slope b of the above relation, the errors on $\delta\alpha$ and $\delta log f_{\nu_J}$ must be taken into account, especially if they differ on the two axes. Errors on $\delta log f_\nu$ for the plate pairs of each band can be computed as follows. From the photometric catalog of the area of sky which has been monitored (KKC,T89,T94,BTK98), each containing 2540 objects brighter than B_J=22.5, we computed $\delta log f_{\nu_J}$ for each object and for each band. Then, in each band, we sorted the objects according to their magnitude, and for each object we took the 100 nearest neighbors (in magnitude) and computed the r.m.s. value σ_{δ_i} of $\delta log f_{\nu_i}$ (i=U, B_J, F, N), after the exclusion of the points lying more than three standard deviations from the mean. As most of the objects in the field are non-variable we assume σ_{δ_i} as a measure of the r.m.s. photometric noise on the flux differences δf_{ν_i}. Using the entire plate set, consisting of 5, 15, 5, 6 plates in the U, B_J, F, N bands respectively, it is also possible to derive a magnitude dependent photometric error for each plate (instead of considering the error on the magnitude difference in plate pairs).

As above we sorted the 2540 objects according to their B_J magnitude (on some reference plate), then for each object we considered the light curve, its time average and its mean square dispersion, in each band. Then we took 100 neighboring objects in magnitude and computed the r.m.s. dispersions around the time average. Neglecting the variance of the time average, this provides an estimate of the r.m.s. photometric error of individual plates. The errors estimated from plate pairs are consistent with a quadratic combination of the errors of the relevant individual plates. These errors are shown for each point of Figure 3.

The variance of $\delta\alpha$ is a linear combination of the variances of the signals in the bands involved, with appropriate coefficients depending on the frequencies of the bands. We can fit to the $\delta\alpha$,$\delta log f_{\nu_J}$ data a straight line taking into account the errors of individual points on both axes. The actual calculation is done using the "fitexy" subroutine from (Press & Teukolsky 1992), which gives also the statistical uncertainties on a and b. The result, with one sigma errors, is $a = (-8.49 \pm 5.50)10^{-2}$ and $b = (2.55 \pm 0.75)$.

Repeating the analysis with the exclusion of the N band reduces the effect of a deviation of the SED from a power low providing a less biased, but more noisy, estimate of the local spectral slope. The correlation is lower, but still positive and marginally significant ($\rho = 0.27, P(> \rho) = 8.87 \cdot 10^{-2}$). The straight line fit to the data, $a = (-1.67 \pm 3.07)10^{-3}$ and $b = 2.29 \pm 0.37$, is quite consistent with the previous result.

Di Clemente et al. 1996 found that the average increase of variability with redshift is $\Delta S_1/\Delta\log(1+z) \simeq 0.25 - 0.30$. This quantity is related to the slope b by: $\Delta S_1/\Delta\log(1+z) \simeq \Delta S_1/\Delta\log\nu \simeq \langle\delta\alpha^2\rangle^{1/2} \simeq b\ \langle(\delta\log f_\nu)^2\rangle^{1/2}$, where $\langle\delta\alpha^2\rangle^{1/2}$ is the r.m.s. fluctuation of the spectral slope and S_1 is the variability indicator defined in Di Clemente et al. 1996 and $\langle(\delta\log f_\nu)^2\rangle^{1/2} \simeq 0.1$ is the r.m.s. flux density fluctuation. Thus the value of b found in the present analysis is consistent with the increase of variability with frequency found by Di Clemente et al. 1996 and confirms the interpretation of the positive v-z correlation suggested by GTV , by a direct observation of the r.m.s. slope variability. We can compare our statistical results with the $\alpha - log f_\nu$ relation found by Edelson et al. 1990 in individual objects through the analysis of IUE observations. All of their 6 objects have low redshift and are sampled around a wavelength $\lambda \simeq 2000$ Å which is about the average wavelength of our sample ($< z >= 1.365$). For 5 of their objects they find a significant correlation of α and $log f_{nu}$. For 4 of these objects the slope b of the relation $\alpha = b\ log f_\nu + const$ is around 1.7, while 3C 273 shows a steeper ($b \approx 2.8$) relation.

It would also be interesting to compare our findings with the variability of (B-R) colors measured by Giveon et al. 1999 in a sample 42 of PG QSOs. Although the average redshift and the rest-frame wavelength region sampled, $< z > \simeq 0.12$, $\lambda \approx 3500$ Å differ from ours, qualitatively their results agree with ours, namely they also find a hardening of the spectrum during bright phases. A more detailed and quantitative comparison requires a re-analysis of Giveon et al. 1999 data in a consistent way (Trevese & Vagnetti, in preparation; Trevese & Vagnetti 2000a,b).

4. Discussion and Summary

Let us assume that the SEDs of the objects of our sample are typical of QSOs, namely they are dominated by the big blue bump in the spectral region around $\lambda = 2000$ Å (see e.g. Bregman 1990). We want to check the hypothesis that both the SED slope and brightness changes are caused by temperature changes of an emitting black body. For this purpose we use U, B_J, F data only and we assign the slope α to the intermediate frequency $log\overline{\nu} = \frac{1}{3} log(\nu_U \nu_J \nu_F)$. Figure 5 shows α versus $\log \bar{\nu}$ for each object. In the same figure the curves $\alpha(x) \equiv 3 - xe^x/(e^x - 1)$, $x \equiv h\nu/kT$, of black bodies are also reported, for various values of the temperature T, h and k being the Planck and the Boltzmann constants.

EDITOR: PLACE FIGURE 5 HERE.

The two points marked with stars represent the uncorrected SED of the two highest redshift objects, which are affected by the intergalactic Ly-α absorption and appear particularly steep. Since SA 57 is close to the Galactic pole, interstellar reddening has a negligible effect on the location of points in Figure 5. The distribution of α is skewed towards negative values, with most objects around -0.5. To check the consistency of slope and brightness variation in a more stringent way, we exclude from the sample the most deviant points, with $\alpha < -2\sigma_\alpha$. Then we obtain $< \alpha >= -0.48 \pm 0.68$. The corresponding average temperature is $T \approx 25000K$. We cannot compare $\delta\alpha/\delta log f_{\bar{\nu}}$ with α of individual objects because the noise is too large, especially on the former quantity. However we can compare the slope b of the straight line fitting the points in Figure 4, representing the average increase of the spectral slope α for increasing luminosity, with the corresponding relation expected for black body spectra of varying temperature. Brightness and slope variations of the SED of a black body of fixed surface are related by $(d\alpha/dT)/(dlogB_\nu/dT) = (\ln 10)[1 - x/(e^x - 1)] \equiv F_{BB}(x)$. In Figure 6, $F_{BB}(x)$ and $\alpha(x)$ are plotted as functions of x.

EDITOR: PLACE FIGURE 6 HERE.

The value of $< \alpha >$ and the r.m.s. spread σ_α of the sample define an interval of x in this plot. In the same figure is also reported the value of b and $(b - \sigma_b)$ as deduced from the statistical analysis of section 2, which define a lower limit on x.

As seen from Figure 6, the above values define a non-empty region of consistency between $F_{BB}(x)$ and $\alpha(x)$ for the sample. A black body with $x \approx 3$ satisfies simultaneously the two constraints. Thus we can say that the $\delta\alpha$ and $\delta log f_{\nu_J}$, observed at an average rest-frame $\bar{\lambda} \approx 2000$ Å are consistent with temperature variations of a typical black body of temperature $T \approx 25000K$.

A single black-body spectrum is an oversimplified representation of the SED which, in the case of accretion disks models, ignores temperature gradients and the presence of other components necessary to explain the emission outside the frequency range considered. In any case we can say that:

i) The increase of the amplitude of variability with the rest-frame frequency (Giallongo, Trèvese & Vagnetti 1991, Cristiani et al. 1996, Di Clemente et al. 1996) is due to the hardening in the bright phases (and vice versa) of the spectrum, which to a first approximation maintains its local power-law shape.

ii) The r.m.s. slope variations are quantitatively consistent with the increase of variability for increasing frequency found by Di Clemente et al. 1996. This confirms, by a direct observation of spectral slope changes, that correlation between the variability and redshift is accounted for by intrinsic spectral changes and does not require cosmological evolutionary effects.

iii) Our results show that the average changes of the SED slope and the relevant flux variations in the optical-UV region are at least not inconsistent with temperature variations of a single emitting black body of $T \approx 2.5 \cdot 10^4 K$.

iv) The average relation between slope and brightness variations provides a new constraint on models of the emission mechanism.

For instance, an optically thin plasma model (Barvainis 1993) requires a temperature of the order of $10^6 K$ to explain with a single emission component the SED from optical-UV to X-ray frequencies (see Fiore et al. 1995). The bremsstrahlung luminosity $L_\nu \propto T^{-1/2} e^x$ (Rybicki & Lightman 1979), can provide an optical-UV spectral slope α consistent with the observations, but in this case the slope and brightness changes produced by temperature changes are related by $F_{ff}(x) \equiv \partial\alpha/\partial log f_\nu = x/(x-1/2)$, i.e. $F_{ff} \simeq -2x$, for $x \ll 1$. Thus, for $T \approx 10^6$, $F_{ff} \approx -0.1$ is not only too small in absolute value, but it is even negative, thus completely inconsistent with the result of our analysis. Notice that also the temperature changes of a simple black body of $T \approx 10^5 K$ would be inconsistent with our findings since, for $\lambda \approx 2000$ Å, this temperature implies $F_{BB} \simeq 0.27$. In fact, at high temperature any thermal emission approaches the limit where the long-wavelength part has a fixed spectral slope, independent of temperature changes (Paltani and Courvoisier 1994). Any model trying to reproduce the observed SED from the IR to X-rays could be tested against the observed $\alpha - log f_\nu$ relation. In particular, it is possible to investigate whether the variation of one, or some, of the parameters involved (like the temperature) are capable of reproducing the observed relation. Perhaps additional phenomena, e.g. hot spots or flares (Krishan & Wiita 1994, Kawaguchi et al. 1998) over an otherwise stationary accretion disk, are needed to explain the SED variability. The main limit of the present analysis are the small amplitude of variability, due to the short time interval (1 yr) between the observations, and the lack of $\alpha - log f_\nu$ relation for individual objects, which could be different depending, e.g., on their intrinsic luminosity.

Despite these limits, our results clearly show that a few additional multi-band observations, properly distributed in time, could provide strong constraints on the physics of emission and variability, especially if associated with simultaneous observations in the IR and X-rays.

This work was partly supported by the Italian Ministry for University and Research (MURST) under grant Cofin98-02-32

REFERENCES

Angione, R. J., & Smith, H. J., 1972, in IAU Symp 44, External Galaxies and Quasi-Stellar Objects, ed. D. S. Evans, (New York: Springer-Verlag), p.171

Aretxaga, I., & Terlavich, R., 1994, MNRAS, 269, 462

Aretxaga, I., Cid Fernades, & Terlavich, R., 1997, MNRAS, 286, 271

Barvainis, R. 1993, ApJ, 412, 513

Bershady, M. A., Trèvese, D., & Kron, R. G. 1997, ApJ, 496, 103 (BTK)

Bregman, J. N. 1990, A&A Rev., 2, 125

Cristiani, S., Vio, R., & Andreani, P. 1990, AJ, 100, 56

Cristiani, S., Trentini, S., La Franca F., Aretxaga, I., Andreani, P, Vio, R., & Gemmo A. 1996, A&A, 306, 395

Cutri, R. M., Wisniewski, W. Z., Rieke, G. H., & Lebofski, H. J. 1985, ApJ, 296, 423

Di Clemente A., Natali G., Giallongo E., Trévese D., Vagnetti F. 1996, ApJ, 463 466.

Edelson, R. 1992, ApJ, 401 516

Edelson, R.A., Krolik, J. H.,& Pike, G. F. 1990, ApJ, 359, 86

Fiore, F., Elvis, M., Siemiginowska, A., Wilkes, B.J., McDowell, J.C., & Mathur, S.: 1995, ApJ449 74

Giallongo, E., Gratton, R., Trèvese, D. 1990, MNRAS, 244, 450

Giallongo E., Trèvese D., Vagnetti F.: 1991, ApJ377 345.

Giveon, U., Maoz, D., Kaspi, S., Netzer, H., & Smith P. S. 1999, MNRAS, 306, 637

Green, A. R., McHardy, I. M., & Letho, H. J., 1993, MNRAS, 265, 664

Kawaguchi, T., Mineshige, S., Umemura, M., & Turner, E. L. 1998, ApJ, 504, 671

Kinney, A. L., Bohlin, R.C., Blades, J. C., & York, D. G. 1991, ApJS, 75, 645

Hawkins, M. R. S. 1983, MNRAS, 202, 571

Hawkins, M. R. S., 2000, A&AS, 143, 465

Hawkins, M. R. S., & Véron, P. 1993, MNRAS, 260, 202

Hawkins, M. R. S., & Véron, P. 1996, MNRAS, 281, 348

Hook, I. M.,McMahon R. G., Boyle, B. J., & Irwin, M. J. 1994, MNRAS, 268, 305

Koo, D. C. 1986, ApJ, 311, 651

Koo, D.C., Kron, R.G., Cudworth K.M.: 1986, PASP, 98, 285 (KKC)

Koo, D. C., & Kron, R. G. 1988, ApJ, 325, 92

Kaspi, S., Smith, P. S., Netzer, H., Maoz, D., Jannuzi, B. T., & Giveon, U., 2000, ApJ, 533, 631

Krishan, V., & Wiita, P. J. 1994, ApJ, 423, 172

Kron, R. G., & Chiu, L. -T. 1981, PASP, 93, 397

Majewski, S. R., Munn, J. A., Kron, R. G., Bershady, M. A., Smetanka, J. J., & Koo, D. C. 1991, in ASP Conf. Proc. 21, The Space Distribution of Quasars, ed. D. Crampton (San Francisco: ASP), 55

Massaro, E., & Trèvese, D. 1996, A&A, 312, 810

Massaro, E., Nesci, R., Maesano, M, Montagni, F, Trèvese, D. et al. 1996, A&A, 314, 87

Munn, J. A.,Koo, D. C.,Kron, R. G., Majewski,S. R., Bershady, M. A., & Smetanka, J. J. 1997, ApJS, 109, 45

Mushotzki, R. F., Done, C., & Pounds, K. A. 1993, ARA&A, 31, 717

Miyaji, T., Connoly, A. J., Szalay, A. S., & Boldt, E. 1997, A&A, 323, L37

Paltani, S., & Courvoisier, T. J.-L. 1994, A&A, 291, 74

Pica, A. J., & Smith, A. G., 1983, ApJ,272, 11

Press, W. H., & Teukolsky, S. A. 1992, Computers in Physics, 6, 274

Rees, M. 1984, ARA&A, 22, 741

Rybicki, G. B., & Lightman, A. P. 1979, Radiative Processes in Astrophysics, John Willey & Sons, New York

Steidel, C. C., & Sargent, W. L. W. 1987, ApJ, 313, 171

Trèvese, D., Kron, R. G., Majewski, S. R., Bershady, M. A., Koo, D. C. 1994, ApJ, 433, 494 (T94)

Trèvese D., Pittella G., Kron R. G., Koo D. C., & Bershady M. A. 1989, AJ98 108. (T89)

Trèvese, D., & Vagnetti, 2000a to be published in proc. Guillermo Haro Advanced Lectures on the Starburst-AGN Connection, Tonantzintla, Mexico, June 26-30 2000, astro-ph/0011076

Trèvese, D., & Vagnetti, 2000b proc. 4th Italian Meeting on AGN "AGN nel 2000", Trieste, May 15-18, 2000, to be published in Mem. SAIt , astro-ph/0007161

Ulrich MH, Maraschi L., & Urry C. M. 1997, ARA&A, 35, 445

Uomoto, A. K., Wills, B. J., & Wills, D., 1976, AJ81, 905

This manuscript was prepared with the AAS LaTeX macros v4.0.

Fig. 1.— Redshift of all the objects of the sample vs. the apparent magnitude (m_4), defined as the B_J magnitude evaluated in a fixed aperture of radius of 1".1. The stars represent the two highest redshift objects. The open circles represent the five objects with extended images from BTK. Lines of constant luminosity $M_J = -23$ and $M_J = -21$ are drawn assuming $H_o =\ 50\ km\ s^{-1}Mpc^{-1}, q_o = 0.5, and \alpha = -1$.

Fig. 2.— U, B_J, F flux as a function of the rest-frame frequency, normalized at 2000 Å, for the 40 objects of the sample. The photometric data of the 5 objects from the list of BTK98 are represented by dots.

Fig. 3.— The spectral energy distribution in arbitrary scale. *Filled circles*: first epoch; *open circles*: second epoch. The relevant power-law fits are also shown. The scale is the same for each pair of data sets representing the same objects at two different epochs.

Fig. 4.— $\delta\alpha$ versus $\delta log f_\nu$, with f_ν measured in the B_J band, on independent plates (see text). The dashed lines represent the linear regressions, from which the correlation coefficient ρ is computed. The solid line is the linear fit which takes into the errors in both coordinates.

Fig. 5.— The slope α as a function of $x \equiv h\nu/kT$, for the 40 objects of the sample, as computed from U, B_J, F bands, with $log\nu = \frac{1}{3}log(\nu_U\nu_B\nu_F)$. The stars represent the two highest redshift objects whose colors are affected by Ly$_\alpha$ absorption. The open circles represent the five objects with extended images from BTK. The solid lines represent $\alpha(x)$ for black bodies of different temperatures T, indicated in units of 10^4 K. The horizontal lines represent $< \alpha > \pm\sigma_\alpha$, after the exclusion of the 3 points at more than 2-sigma from the mean.

Fig. 6.— $\alpha(x)$ and $F_{BB}(x)$ for a black body, as a function of $x \equiv h\nu/kT$. The continuous horizontal lines represent respectively $< \alpha >$ and the slope b of the straight line fitting the

data in Figure 3. The dashed and dotted lines represent the one-sigma interval and the relevant bound on x, deriving from the comparison of the data with the black body curves $F_{BB}(x)$ and $\alpha(x)$ respectively.

Table 1. Plate Journal.

MPF #	UT date	Band
3919	1984 Apr 05	B_J
3920	1984 Apr 05	U
3921	1984 Apr 05	B_J
3922	1984 Apr 05	F
3923	1984 Apr 05	N
3973	1985 Apr 25	N
3975	1985 Apr 26	F
3976	1985 Apr 25	U
3977	1985 Apr 25	B_J

TABLE 2

SUMMARY OF OBSERVATIONS

N_{694}	N_{2540}	N_{ser}	KKC	α_{1950}	δ_{1950}	m_4	z	B_J(3919)	U(3920)	B_J(3921)	F(3922)	N(3923)	N(3973)	F(3975)	U(3976)	B_J(3977)
4	11	100360	54	13:06:36.23	29:21:55.8	19.43	0.75	19.70	18.46	19.40	18.71	18.41	18.65	18.66	18.70	19.82
255	902	107624	28	13:05:53.15	29:35:15.9	19.59	1.74	19.40	18.37	19.34	18.74	18.63	18.67	18.90	18.45	19.42
389	1427	111610	22	13:05:48.99	29:41:10.6	19.81	3.02	19.07	19.72	19.33	18.14	18.14	17.97	18.14	19.57	19.04
613	2278	117750	19	13:05:45.60	29:50:46.7	19.87	1.18	19.81	18.83	19.80	19.05	19.10	19.03	19.17	18.95	19.68
563	2138	116713	10	13:05:26.41	29:49:01.7	20.14	0.99	19.62	18.86	19.62	19.03	19.31	19.23	19.12	18.91	19.51
109	412	103544	50	13:06:26.74	29:28:42.3	20.20	0.55	20.75	19.59	20.51	20.44	20.07	20.08	20.41	19.87	21.06
...	51	100681	...	13:05:42.88	29:22:52.4	20.37	0.40	20.25	19.30	20.17	19.75	19.42	19.33	19.70	19.32	20.03
654	2410	118749	55	13:06:41.23	29:52:33.3	20.41	1.09	20.22	19.65	20.26	19.99	20.02	19.97	19.86	19.84	20.28
254	899	107567	37	13:06:09.20	29:35:09.7	20.60	1.81	20.83	20.20	20.82	20.68	20.35	20.34	20.85	20.24	20.95
160	606	105141	34	13:06:04.31	29:31:23.1	20.62	1.09	20.83	20.01	20.78	20.41	20.49	20.52	20.30	19.85	20.61
187	686	105767	...	13:05:15.05	29:32:25.0	20.73	0.71	20.79	20.62	20.77	20.00	19.32	19.38	20.11	20.64	20.78
172	641	105422	64	13:06:49.05	29:31:49.7	20.76	1.08	19.73	18.99	19.76	19.44	19.42	19.89	19.71	19.44	19.87
...	1821	114264	...	13:05:40.52	29:45:07.1	20.77	0.29	20.66	20.92	20.72	19.01	18.41	18.23	19.19	20.62	20.43
335	1184	109980	25	13:05:50.30	29:38:42.1	20.78	1.55	20.71	19.87	20.72	20.60	20.38	20.29	20.69	20.07	20.74
30	88	101012	32	13:06:02.22	29:23:44.1	21.01	2.28	20.36	19.99	20.30	20.14	20.11	20.59	20.55	20.11	20.55
459	1772	113966	46	13:06:21.32	29:44:37.6	21.09	0.95	20.96	20.14	21.04	20.84	20.51	20.95	20.99	20.31	21.11
42	130	101339	44	13:06:17.75	29:24:33.3	21.15	0.00	21.05	20.50	21.01	20.76	20.53	20.62	20.91	20.58	21.17
240	856	107326	43	13:06:16.89	29:34:48.1	21.17	0.59	20.95	20.19	20.89	20.63	20.09	20.15	20.39	19.94	20.62
40	121	101304	11	13:05:27.05	29:24:30.0	21.21	2.27	20.98	20.56	20.98	20.93	21.60	21.78	21.24	21.11	21.27
371	1363	111178	...	13:07:23.27	29:40:29.6	21.32	1.61	21.65	20.98	21.48	21.45	20.49	20.81	21.08	20.89	21.50
...	512	104326	...	13:06:30.80	29:30:04.3	21.33	0.21	21.15	20.88	21.06	20.51	20.37	20.22	20.52	20.85	21.20
...	1210	110195	...	13:05:10.46	29:39:02.5	21.43	0.24	21.31	20.97	21.33	20.24	19.23	19.36	20.21	20.62	21.02
180	670	105643	27	13:05:52.78	29:32:10.4	21.47	0.98	21.26	20.80	21.19	20.90	22.03	21.71	21.42	21.00	21.37
495	1935	115180	31	13:06:01.51	29:46:34.2	21.53	0.92	20.62	19.88	20.64	20.38	20.09	20.10	20.61	20.06	20.41
153	575	104855	67	13:06:57.73	29:30:55.4	21.55	1.30	22.37	21.33	22.34	22.12	...	21.33	21.52	20.69	21.64
627	2325	118122	63	13:06:47.33	29:51:21.6	21.56	0.68	21.41	20.65	21.45	21.33	21.89	21.66	21.93	21.21	22.10
683	2494	119387	51	13:06:28.60	29:53:56.0	21.86	1.46	22.09	21.18	22.08	22.06	21.99	21.13	21.62	20.68	21.73
114	432	103707	70	13:07:04.00	29:29:03.2	21.88	0.94	21.99	21.11	21.80	21.93	21.48	21.51	21.70	20.75	21.62
152	574	104882	23	13:05:49.22	29:30:57.1	21.92	1.47	21.54	21.15	21.44	21.11	20.71	20.39	21.17	21.16	21.38
91	334	102888	68	13:07:03.68	29:27:43.9	21.96	1.33	21.80	20.69	21.51	21.36	21.19	21.51	21.27	20.79	21.74
274	970	108169	...	13:05:38.70	29:36:07.4	22.04	0.74	21.89	21.74	21.93	21.60	21.13	21.27	21.60	21.55	21.72
44	136	101392	35	13:06:07.48	29:24:41.5	22.16	3.08	22.17	23.38	22.05	21.56	21.86	21.47	21.63	22.93	22.10
261	931	107822	9	13:05:19.62	29:35:34.9	22.17	2.46	21.58	21.03	21.58	21.46	22.63	22.73	21.73	21.05	21.55
384	1400	111450	36	13:06:07.54	29:40:59.5	22.22	0.96	21.88	21.56	21.96	22.13	23.47	22.82	22.17	21.73	22.02
329	1172	109877	30	13:06:00.43	29:38:32.0	22.25	2.12	22.13	21.51	21.97	21.72	20.74	20.56	21.60	21.22	21.71
445	1696	113412	58	13:06:43.56	29:43:45.1	22.26	2.08	22.06	21.35	22.13	22.34	23.36	22.78	22.15	21.30	22.09
...	635	105334	...	13:07:21.35	29:31:44.0	22.36	0.30	22.21	21.61	22.06	21.79	20.69	21.48	21.53	21.77	22.26
208	744	106442	56	13:06:41.93	29:33:26.8	22.39	2.12	21.19	20.53	21.23	21.28	21.36	21.16	21.08	20.47	21.07
333	1178	109934	16	13:05:43.25	29:38:36.9	22.43	2.53	21.03	20.95	21.11	21.25	20.87	21.33	21.56	21.20	21.42
338	1189	110028	1	13:04:49.59	29:38:45.8	22.51	0.65	22.35	21.49	22.44	22.22	22.02	21.00	22.25	21.43	22.20

NOTE.– N_{694} is the serial number of point-like objects in T89, N_{2540} refers to the catalog described in BTK, N_{ser} is the serial number of the matching objects in the catalog of Koo 1996 as reported by Munn et al. 1997 and KKC is the serial number in Koo, Kron, & Cudworth 1986. The magnitude m_4 in column 7 is computed in a circular aperture of 1".1 on the B_J plate MPF1053 as in T89 and. The redshifts z are taken from T89 and T94. Columns from 9 to 17 contain the magnitudes in the same aperture of 1".1 of m_4 obtained from the indicated plates.

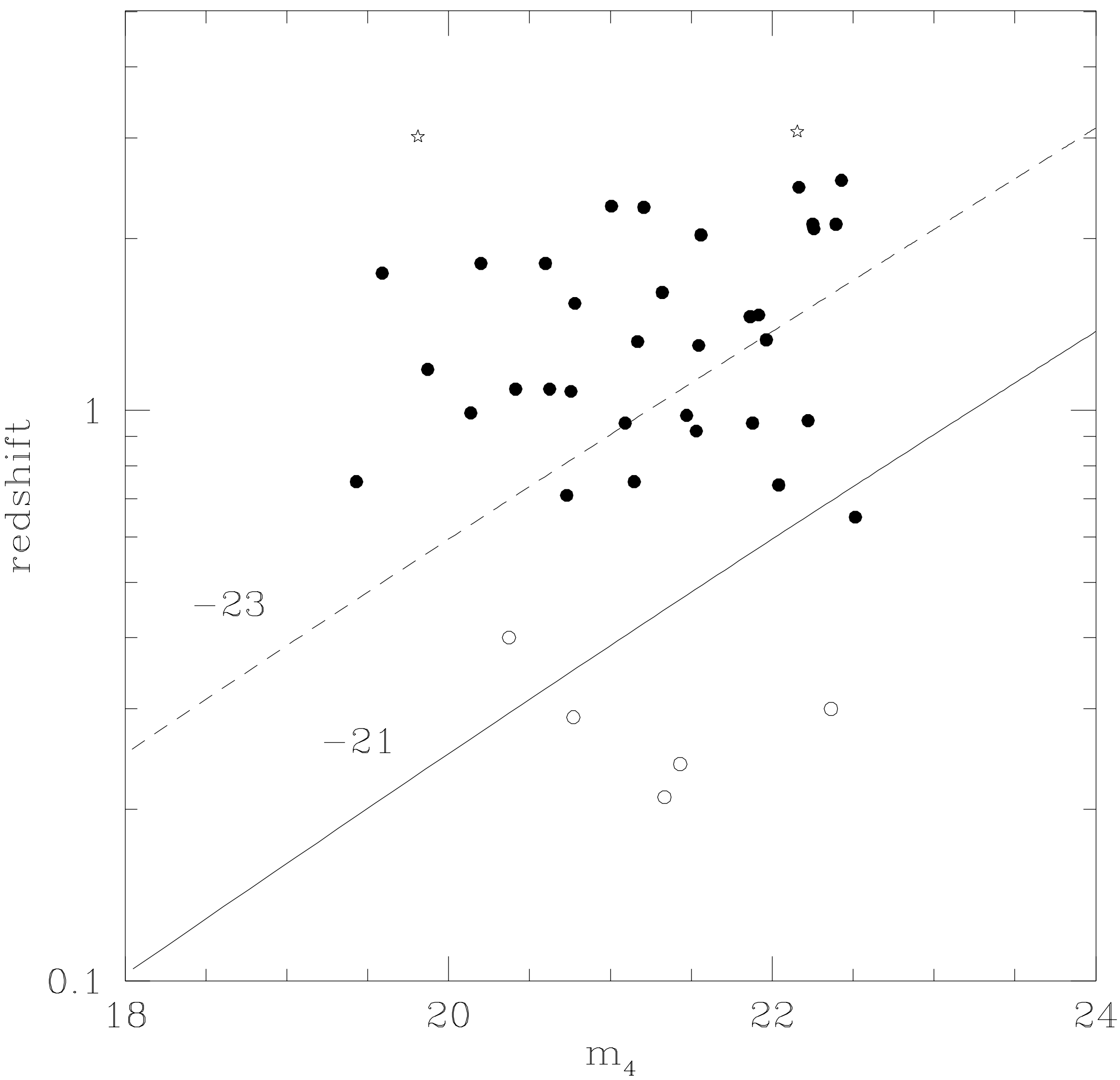
redshift
1
0.1
18
20
22
24
m$_4$
−23
−21

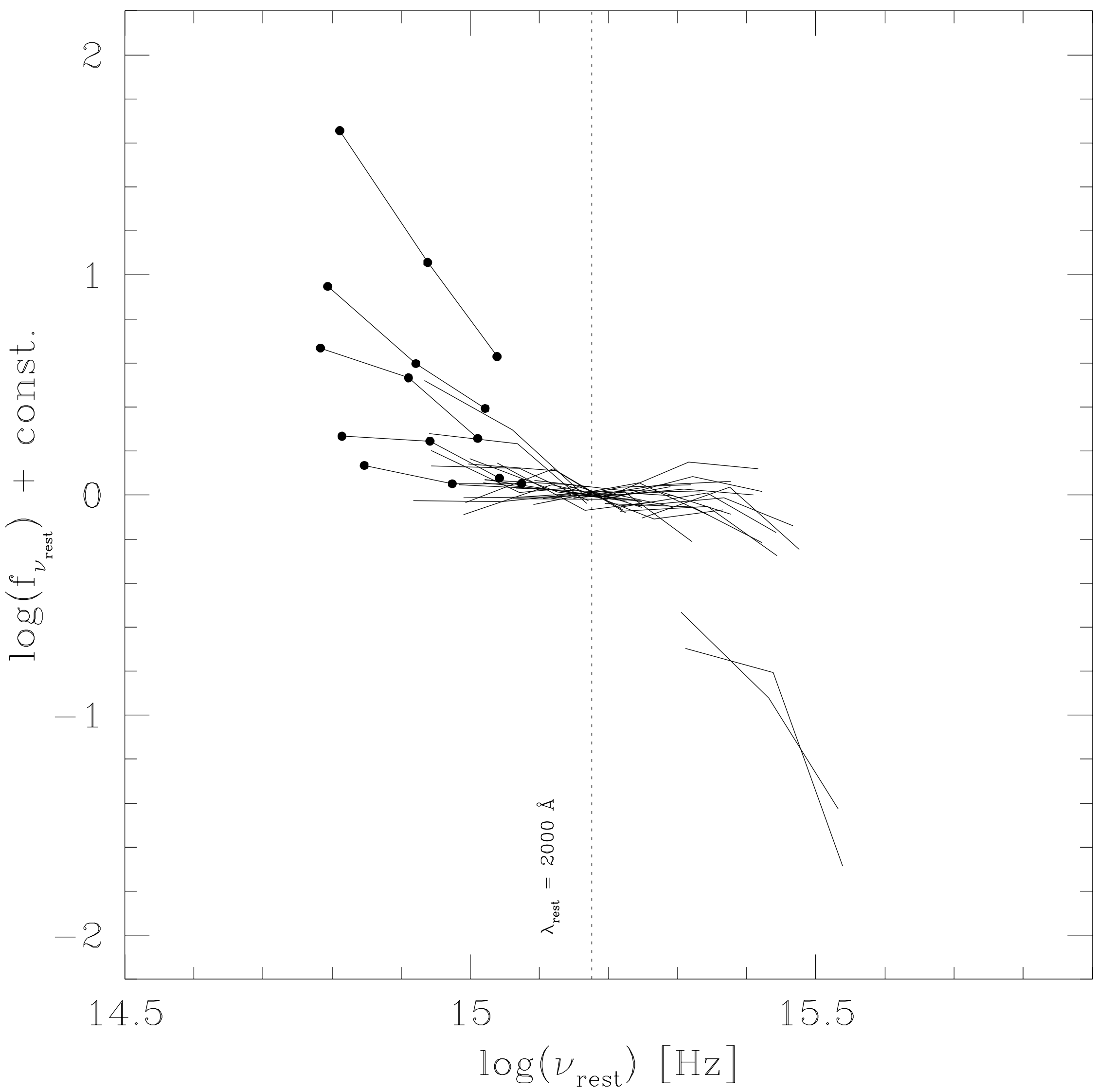
2
1
0
−1
−2
14.5
15
15.5
log($f_{\nu_{rest}}$) + const.
log(ν_{rest}) [Hz]
λ_{rest} = 2000 Å

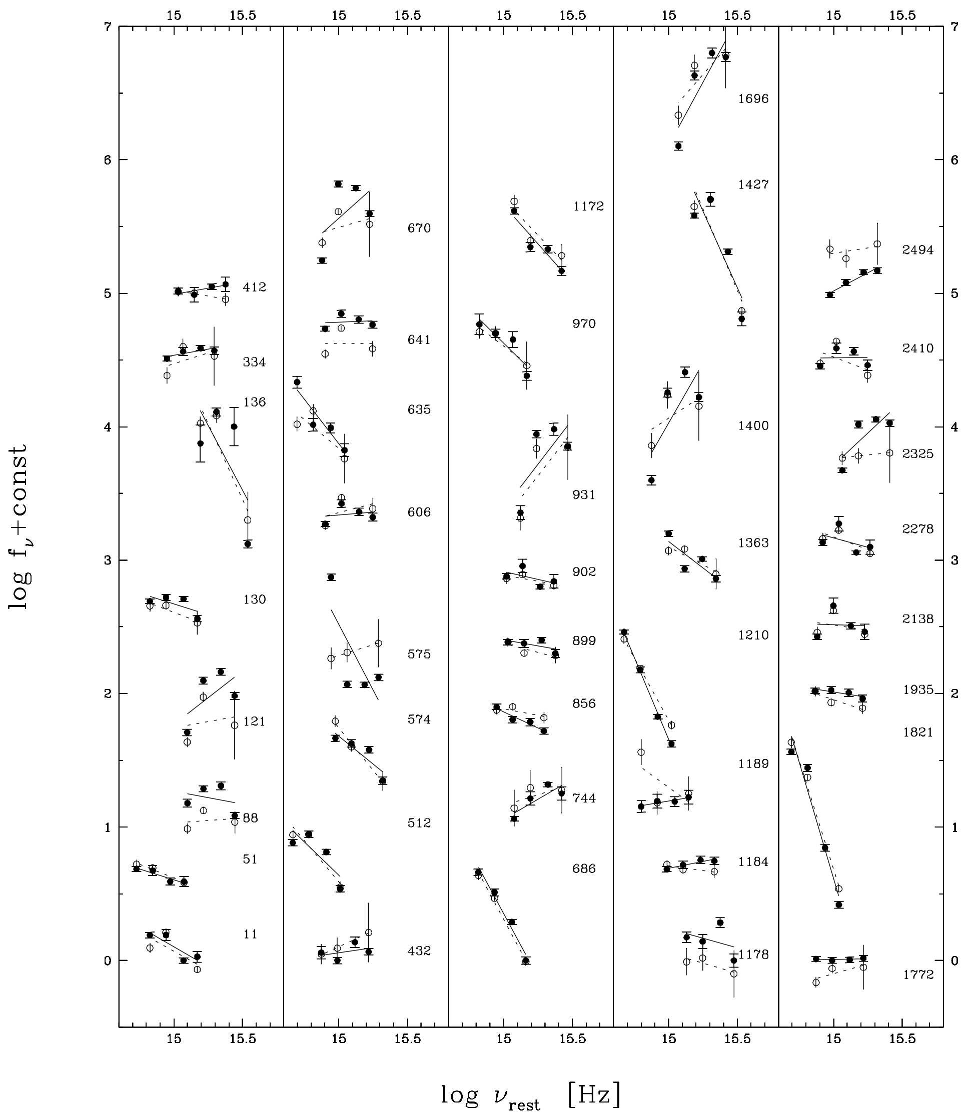

log f$_\nu$+const
log $\nu_{\rm rest}$ [Hz]
15
15.5
0
1
2
3
4
5
6
7
412
334
136
130
121
88
51
11
670
641
635
606
575
574
512
432
1172
970
931
902
899
856
744
686
1696
1427
1400
1363
1210
1189
1184
1178
2494
2410
2325
2278
2138
1935
1821
1772

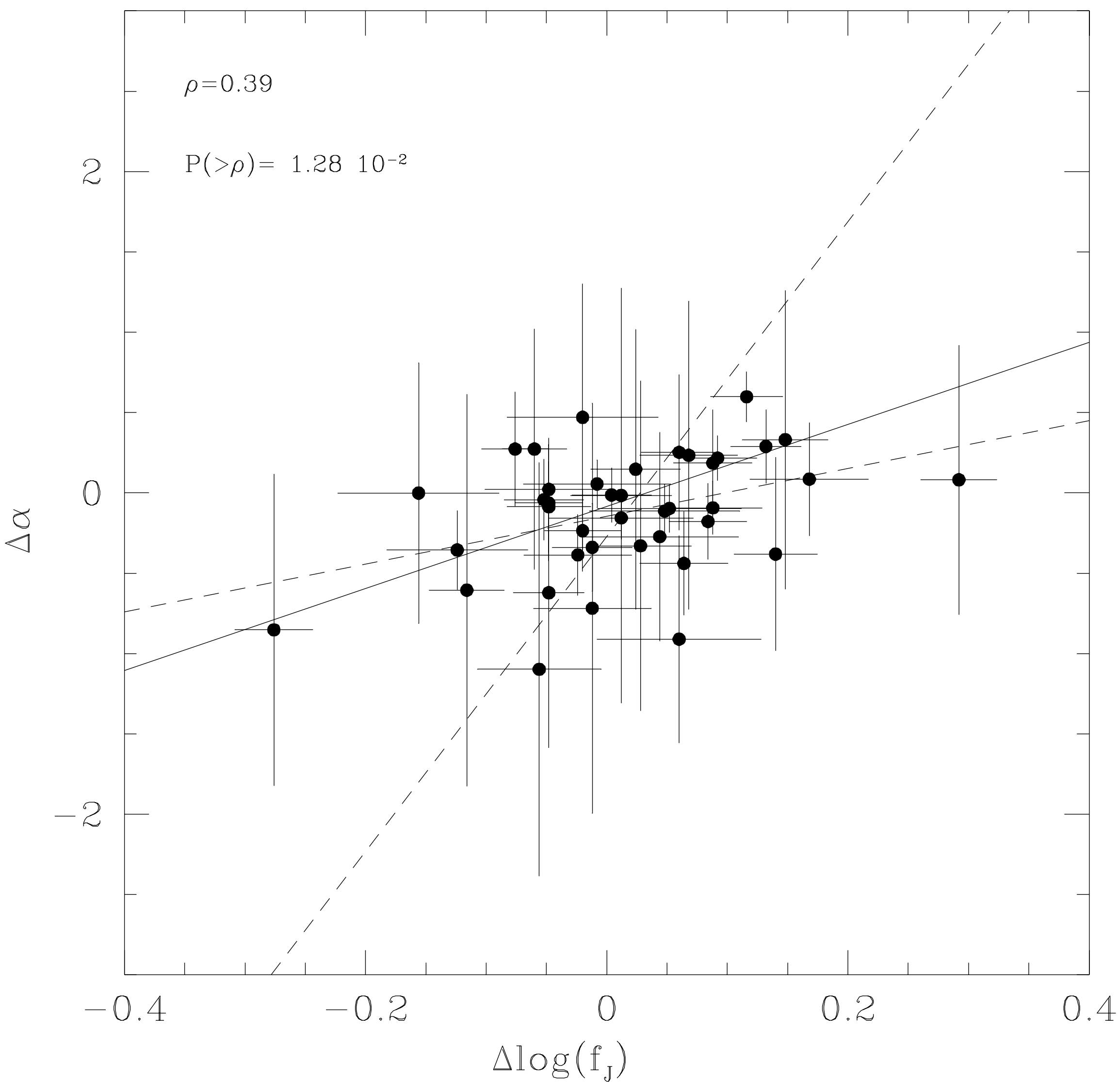
ρ=0.39
P(>ρ)= 1.28 10⁻²
2
0
−2
−0.4
−0.2
0
0.2
0.4
Δα
Δlog(f_J)

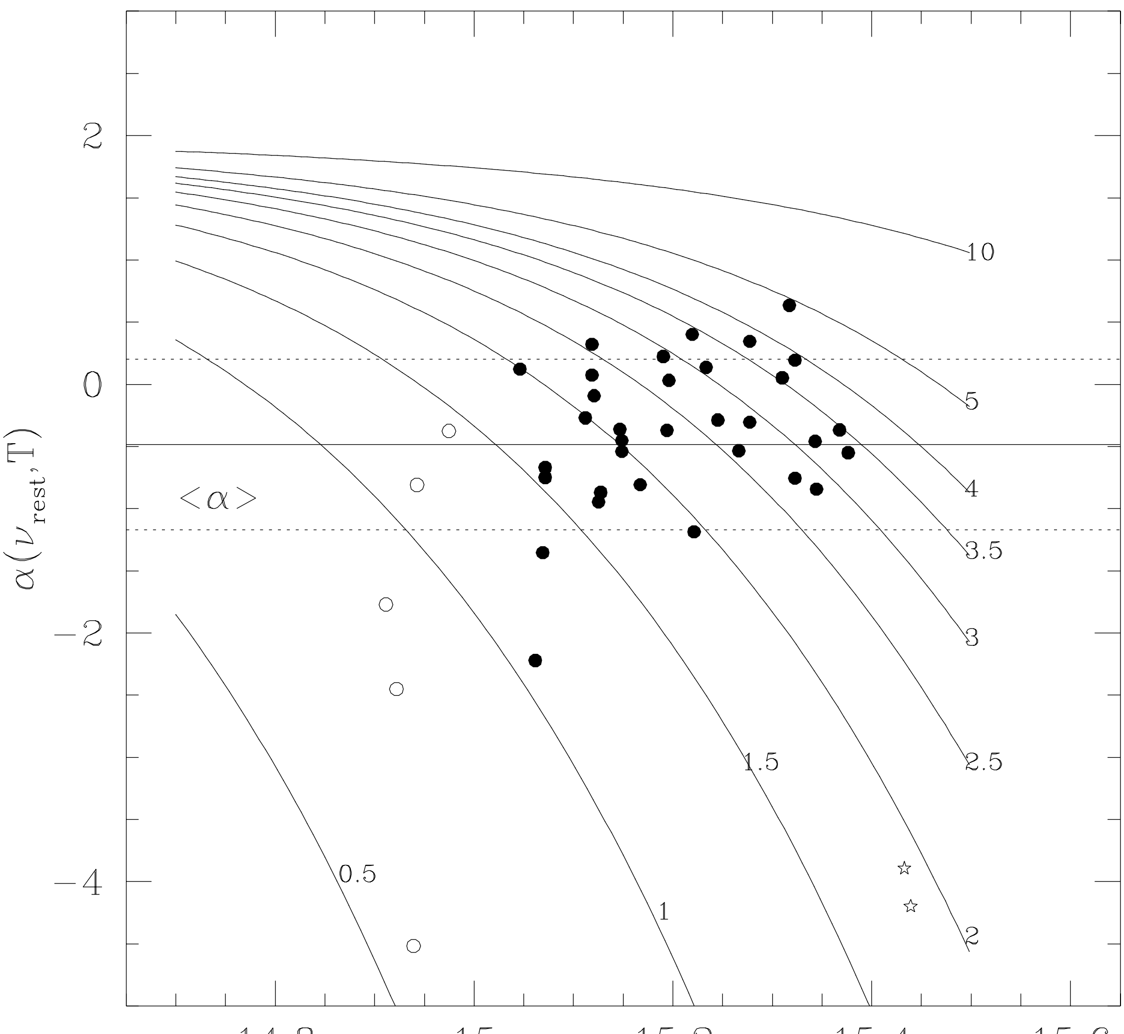

2
0
−2
−4
14.8
15
15.2
15.4
15.6
log $\nu_{\rm rest}$ [Hz]
$\alpha(\nu_{\rm rest},{\rm T})$
$<\alpha>$
10
5
4
3.5
3
2.5
2
1.5
1
0.5

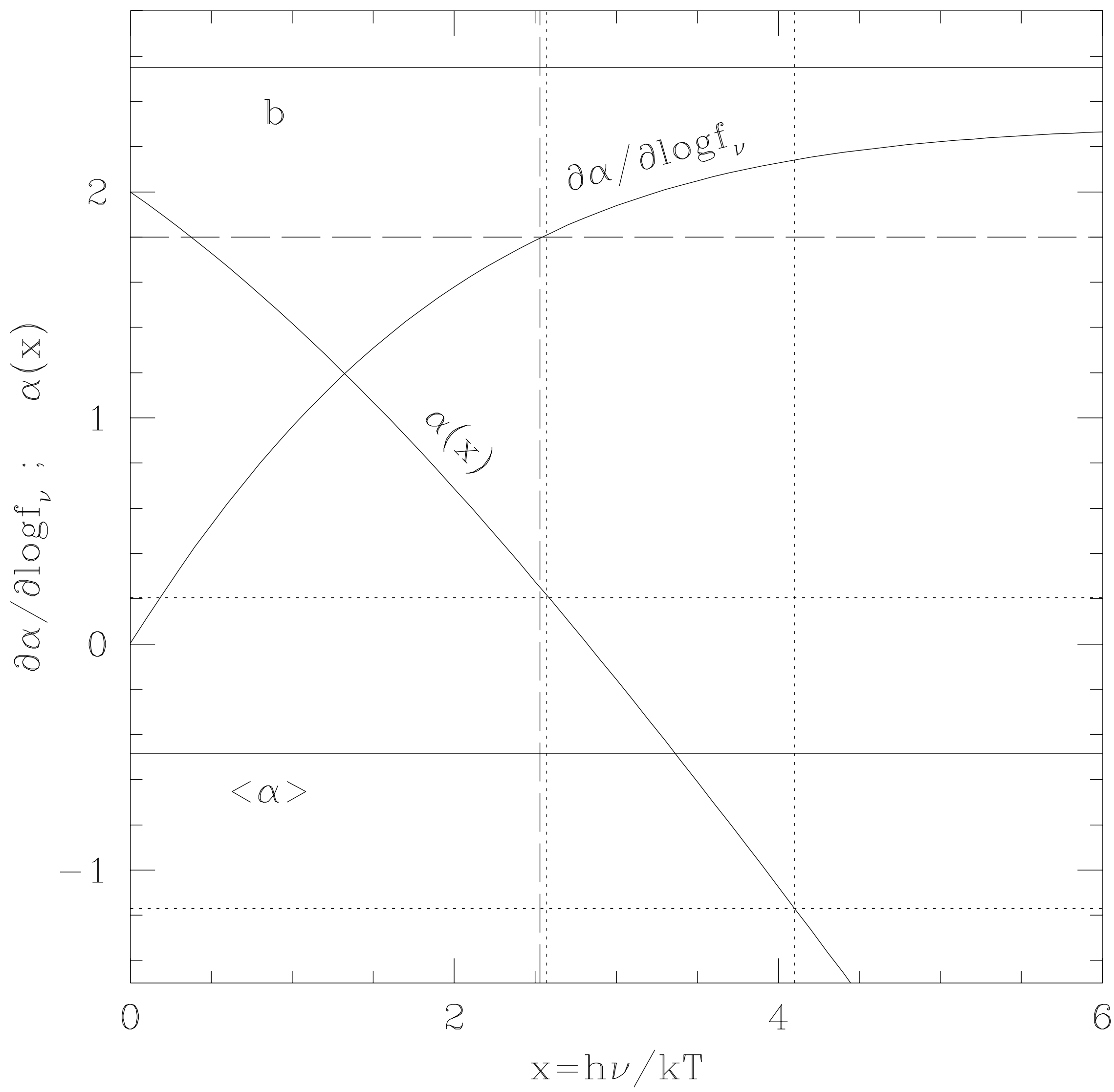

b
∂α/∂logf_ν
α(x)
<α>
∂α/∂logf_ν ; α(x)
0
1
2
−1
0
2
4
6
x=hν/kT